Journal of Wind Engineering & Industrial Aerodynamics 177 (2018) 366–375

Contents lists available at ScienceDirect

Journal of Wind Engineering & Industrial Aerodynamics

journal homepage: www.elsevier.com/locate/jweia

First passage time as an analysis tool in experimental wind engineering

H. Vanvinckenroye [a,b,*], T. Andrianne [c], V. Denoël [a]

[a] Structural Engineering Division, Faculty of Applied Sciences, University of Liège, Liège, Belgium
[b] FRIA (F.R.S.-F.N.R.S), National Fund for Scientific Research, Brussels, Belgium
[c] Wind Tunnel Laboratory, Faculty of Applied Sciences, University of Liège, Liège, Belgium

ARTICLE INFO

Keywords:
First passage time
Wind tunnel experiments
Tower crane
Stochastic Mathieu oscillator
First passage time algorithm

ABSTRACT

The first passage time is the time required for a system to evolve from an initial configuration to a certain target state. This concept is of high interest for the study of transient regimes which are widely represented in wind engineering. Although the concept has been widely studied from theoretical and numerical standpoints, there are very few practical or experimental applications where the results are seen from this angle. This work is a first attempt at bringing first passage times of stochastic systems into wind engineering by suggesting the use of a first passage time map as a standard analysis tool in experimental wind engineering. The wind tunnel data related to the spinning dynamics of a rotating square cylinder in turbulent flow is processed under the frame suggested by a theoretical model for a simple linear oscillator. A specific algorithm is developed for the determination of the average first passage time as a function of initial and target conditions based on the experimental measurements. It is shown that the simple theoretical model is able to capture the different regimes of the experimental setup, so that an equivalent linear Mathieu oscillator, presenting the same evolution of energy, from a first passage time point of view, was identified. This experimental investigation provides a first link between an analytical but simplified result and a more complex reality.

1. Introduction

The first passage time is the time required for a system, leaving a known initial configuration, to reach a certain state for the first time. In deterministic dynamics this concept is central in the description of transient regimes, for instance to estimate the time required for a deterministic system to reach its steady-state, under a stationary excitation (Chopra, 2007). The first passage time has attracted much more attention in a stochastic context, in which numerous theoretical approaches to its estimation and description have been developed (Grigoriu, 2002; Lin and Cai, 2004; Preumont, 1994; Schuss, 2010; Bolotin, 1984; Stratonovitch, Silverman). Although the concept has been widely studied from theoretical and numerical standpoints, there are very few practical or experimental applications where the results are seen from the angle of first passage times. This seems paradoxical for slightly damped and randomly excited structures, such as those which are studied in wind engineering today. Indeed, slightly damped systems have long memory times and require a lot of time before a steady regime can be reached. Because they spend most of their time in transient regimes, it is important to focus on a transient representation of their response. Among others, first passage times are one way to do this.

Some examples of the possible application of first passage times in wind engineering are the following ones. First, dispersion of pollutant releases is the object of massive experimental and numerical research. Reliable and accurate results are obtained through costly high-resolution developments or experimental testing such as field measurements (Barad, 1958; Stathopoulos et al., 2004), atmospheric boundary layer flow simulations (Stathopoulos et al., 2004; Halitsky, 1963; Huber and Snyder, 1982; Li and Meroney, 1983; Meroney, 2004) or computational fluid dynamics (Meroney, 2004, 2016; Gousseau et al., 2011; Tominaga and Stathopoulos, 2013, 2016; Di Sabatino et al., 2013). A bridge deck flutter instability in turbulent flow (Andrianne and de Ville de Goyet, 2016) is another problem in which first passage times are of outmost concern. Another example concerns tower cranes that are left free to rotate as a weathervane in a turbulent wind velocity field. The increasing number of recorded accidents due to high wind and partly to the autorotation (Mok, 2008) aroused the curiosity of the scientific community. Out-of-service wind velocities criteria are proposed by (Eden et al., 1983; Sun et al., 2009) while the stochastic response under turbulent wind conditions was the object of experimental testing assessing the risk of autorotation of the crane in a given environment (Voisin, 2003; Voisin et al., 2004; Eden et al., 1981, 1983). In all these applications, the

* Corresponding author. Structural Engineering Division, Faculty of Applied Sciences, University of Liège, Liège, Belgium.
E-mail address: hvanvinckenroye@uliege.be (H. Vanvinckenroye).

https://doi.org/10.1016/j.jweia.2018.03.032
Received 5 November 2017; Accepted 30 March 2018

question of first passage time is typically central and offers an alternative answer to the risk assessment with a good understanding of the influence of problem parameters of a system/structure's transient response. In particular it tackles questions such as the time it takes for a pollutant to reach a given concentration at a given place, the time required before stochastic instability occurs, the time it takes for a crane to exhibit large amplitude oscillations, or complete autorotations. The large number of potential applications in wind engineering encourages the development of reliable tools for the understanding and prediction of systems in transient regimes.

We restrict the current study to linear oscillations around an equilibrium point. In a single degree-of-freedom case, a very general model of a linear system, which is also suitable to capture many features of the aeroelastic loading, is composed of inertial, viscous and restoring forces, as well as a forcing and, possibly, a parametric excitation. The stochastic analysis of such systems has been widely studied. In particular, by analogy with a pendulum subjected to a support motion, the stochastic stability of a simple oscillator has already been studied under deterministic or stochastic excitations (Gitterman, 2010a, 2010b; Alevras et al., 2013; Yurchenko et al., 2013). The separatrix between stable and unstable zones is studied in (Bishop and Clifford, 1996; Clifford and Bishop, 1994; Garira and Bishop, 2003; Xu and Wiercigroch, 2006) while (Mallick and Marcq, 2004) provides an asymptotic solution for the probability density function of the energy. Beside, the analysis of non-stationary problems can be done in several different ways, (i) either through Monte Carlo simulations (Kloeden and Platen, 1992; Primožič, 2011; Giles, 2008; Vanvinckenroye and Denoël, 2015) providing for instance the time evolution of the joint probability density function in transient and, eventually, stationary regimes, (ii) either through a more theoretical context, where the state-variable probability density function and the first passage time are obtained as the solutions of the Fokker-Planck-Kolmogorov and generalized Pontryagin equations. These equations can be solved numerically through a path integration method (Kougioumtzoglou and Spanos, 2014a), the perturbation method (Canor et al., 2016), the smooth particle hydrodynamics method (Canor and Denoël, 2013), high dimensional finite elements (Náprstek and Král, 2014, 2017), or other approximate techniques. Comparisons of approached and numerical solutions for the first passage times and the associated, so-called, survival probability, are widely available (Kougioumtzoglou and Spanos, 2014b; Spanos and Kougioumtzoglou, 2014a, 2014b; Palleschi and Torquati, 1989).

Explicit solutions of the Fokker-Planck-Kolmogorov and Pontryagin equations are available in some limited cases only (Chunbiao and Bohou, 2000; Schuss, 2010; Risken, 1996). The stochastic averaging method used in (Vanvinckenroye and Denoël, 2017a, 2017b) to solve the generalized Pontryagin equation provides an approximate but closed-form solution for a single-degree-of-freedom system submitted to broadband parametric and forced excitations. This generic model can be used to describe a wide range of physical problems, such as the behaviour of a tower crane under wind excitation (Vanvinckenroye and Denoël, 2016), the deflection of a cable submitted to an axial oscillation of an anchorage (de Sa Caetano and Engineering, 2007) or ship capsizing and rolling motion (Moshchuk et al., 1995a; Troesch et al., 1992). Although being too simple to capture the full complexity of realistic problems such as those related to colored excitations, non-linearities (Moshchuk et al., 1995b) or multi-degrees-of-freedom structures, it is conjectured that this model can be fitted or adjusted to many (more complex) wind engineering problems. This paper serves as a demonstration, with the particular application of a crane oscillating in a turbulent flow.

While first passage times have been thoroughly studied in many aspects of numerical and theoretical modeling, it is surprising that experimental investigations are very limited. It appears that the only experimental investigations are in the field of applied physics (Roberts and Yousri, 1978; Spano et al., 1989), and usually aim at comparing experimental observations and approached analytical solutions. These applications in other fields of science and engineering suggest that it is a mistake to ignore the first passage time representation of transient signals. Following this motivation, we have decided to process wind tunnel data within the framework of first passage time and to compare the results with the simple theoretical model discussed before. As shown next, results are concluding and suggests the use of first passage time maps as a complementary technique to usual analysis tools (Gurley et al., 1997). This is to the authors' knowledge a first attempt at bringing first passage times of stochastic systems into engineering.

2. A mathematical model of a tower crane

The dynamics of a crane spinning in a turbulent velocity field can be modeled with a governing equation of the type:

$$I\ddot{\theta} + C\dot{\theta} = M_w \tag{1}$$

where $\theta(t)$ is the angular position of the crane jib in a horizontal plane and $M_w(t)$ is the aerodynamic load resulting from the wind flow. Considering that the rotation of the crane is associated with slower timescales than those of the wind flow along a characteristic length of the crane (say its diameter), the quasi-steady assumption (Dyrbye and Hansen, 1997) is considered. The aerodynamic torque is therefore expressed by

$$M_w = \frac{1}{2}\rho_{air} C_M H B^2 ||\boldsymbol{v}_{rel}||^2 \tag{2}$$

as a function of the air density ρ_{air}, the moment coefficient C_M, the circumscribed dimensions of the lattice cross section $H \times B$ (height × span) and the relative wind velocity $\boldsymbol{v}_{rel}$.

There is no angle-proportional term (no stiffness) in the rotative equilibrium (1), since the spinning crane is assumed to be ideally balanced. If the wind was uniform and steady, without turbulence, the crane would find an equilibrium position in the mean direction of the wind; in other words, the stiffness in the problem comes from the aerodynamic loading $M_w(t)$. In this paper, we are concerned with small amplitude rotations of the crane, which also partly justifies a linearized version of the inertial and internal forces in the governing equation, therefore simply modeled by the rotative inertia I and viscosity C.

In the horizontal plane of the crane, the wind velocity is characterized by its mean component U and its fluctuating components u and w respectively parallel and perpendicular to the wind direction (see Fig. 2 (c)), which are stochastic processes characterized by their power spectral densities $\mathcal{S}_u(\omega)$ and $\mathcal{S}_w(\omega)$. For small incidences, the moment coefficient can be linearized too so that $C_M(\alpha) = \frac{\partial C_M}{\partial \alpha}|_{\alpha=0}\alpha$ with α the relative angle between the crane and the instantaneous wind velocity vector. The relative velocity entering in (2) is given by:

$$\boldsymbol{v}_{rel} = (U+u, w) - \left(-r\dot{\theta}\sin\theta, r\dot{\theta}\cos\theta\right). \tag{3}$$

with r the abscissa of the aerodynamic focus along the jib, i.e. the point at which the moment coefficient does not vary with the lift coefficient (Dyrbye and Hansen, 1997). In this model we subscribe to the common assumption that u and w are small compared to U, although they might affect higher order statistics (Dyrbye and Hansen, 1997); also we assume that rotations are small around the equilibrium configuration, i.e. $\theta \ll 1$ and that the rotative velocity of the crane, of order $B\dot{\theta}$ is also small compared to U. The squared norm of the relative velocity and the apparent angle of attack are therefore expressed as

$$||\boldsymbol{v}_{rel}||^2 = U^2 + 2Uu \quad \text{and} \quad \alpha = \theta - \frac{w - r\dot{\theta}}{U} \tag{4}$$

which is identical to usual assumptions for wings (Fung, 2002) and bridge decks (Claudio and Carlotta, 2004; Carlotta and Claudio, 2006).

Respectively grouping together rigidity and damping terms, equation

(1) is rewritten

$$I\ddot{\theta}+\left(C+M^{\star}\frac{r}{U}\left(1+2\frac{u}{U}\right)\right)\dot{\theta}+M^{\star}\left(1+2\frac{u}{U}\right)\theta=M^{\star}\frac{w}{U} \tag{5}$$

where, as soon as $U\neq 0$, the reference torque $M^{\star}$ is defined as

$$M^{\star}=-\frac{1}{2}\rho_{air}HB^{2}U^{2}\frac{\partial C_{M}}{\partial\alpha}>0. \tag{6}$$

As introduced earlier, this quantity also plays the role of a stiffness, aligning the crane with the mean wind orientation $\theta=0$ when there is no turbulence.

A dimensionless version of the governing equation is obtained by introducing the circular frequency of the oscillator $\Omega^{\star}=\sqrt{M^{\star}/I}$ as well as the structural and aerodynamic damping coefficients, $\xi_{s}=\frac{C\Omega^{\star}}{2M^{\star}}$ and $\xi_{a}=\frac{r}{2U}\Omega^{\star}$. It reads

$$\theta''+(2\xi_{s}+2\xi_{a}(1+\tilde{u}))\theta'+(1+\tilde{u})\theta=-\tilde{w}, \tag{7}$$

where symbol $'$ represents a derivative with respect to the non-dimensional time $\tau=\Omega^{\star}t$, and where $\tilde{u}=2\frac{u}{U}$ and $\tilde{w}=\frac{w}{U}$ represent the dimensionless components of the wind fluctuations.

The Hamiltonian of the dimensional system (5) is given by the conservative part of the equation and is defined as

$$H=I\frac{\dot{\theta}^{2}}{2}+M^{\star}\frac{\theta^{2}}{2}=\frac{I}{2}\left(\dot{\theta}^{2}+\Omega^{\star 2}\theta^{2}\right) \tag{8}$$

while the dimensionless Hamiltonian is given by the conservative part of equation (7):

$$\tilde{H}=\frac{\theta'^{2}}{2}+\frac{\theta^{2}}{2}=\frac{H}{M^{\star}}. \tag{9}$$

It is therefore observed that $M^{\star}$ also plays the role of a characteristic energy.

3. Theoretical background for first passage times

A dynamic system like (5) or (7) is stochastic in nature because of the randomness in the fluctuating components of the wind velocity field. Hence, the time required for the system to evolve from a certain initial energy (Hamiltonian) to a higher level of energy, for the first time, is a random variable. The statistical distribution of this *first passage time* can be established by means of numerical simulations (Kougioumtzoglou and Spanos, 2014b; Spanos and Kougioumtzoglou, 2014a, 2014b; Palleschi and Torquati, 1989). As an alternative, analytical expressions of the low order moments can be established in closed form by means of asymptotic approaches, adducing the existence of two different dynamics in the system. In particular, the average (Vanvinckenroye and Denoël, 2017a) and the standard deviation (Vanvinckenroye and Denoël, 2017b) of the first passage time have closed-form expressions, which are well-suited to understand the behaviour of a simple oscillator submitted to broadband excitations.

The use of first passage times in the analysis of slightly damped systems is motivated by the fact that the system memory is long and therefore that steady states take too long to develop. Because the use of first passsage times is novel in wind engineering, some important results are summarized in this Section. They are given in a dimensionless version, in order to ease its later comparison with equation (7). For the sake of simplicity in notations, the tilde symbol is dropped in this Section.

3.1. Undamped oscillator

The undamped, externally and parametrically forced oscillator is governed by the following non-dimensional Mathieu equation:

$$\ddot{x}(\tau)+[1+u(\tau)]x(\tau)=w(\tau). \tag{10}$$

The parametric (multiplicative) and forcing (additive) excitations $u(\tau)$ and $w(\tau)$ are assumed to be δ-correlated noises of spectrum intensity S_{u} and S_{w}, such that $E[u(\tau)u(s)]=\delta(\tau-s)S_{u}$, $E[w(\tau)w(s)]=\delta(\tau-s)S_{w}$ and $E[u(\tau)w(s)]=\delta(\tau-s)S_{uw}$. Assuming that these noises are of small intensity, and that the damping ratio is small, this system spends a large fraction of its time in a transient regime. Another peculiarity is that its total internal energy or *Hamiltonian* $H(\tau)$, defined by $H=\frac{x^{2}}{2}+\frac{\dot{x}^{2}}{2}$ evolves on a slow time scale (Mallick and Marcq, 2004). Let the first passage time τ_{1} be the time required for the system departing from an initial energy H_{0} to reach a target energy $H_{c}=H_{0}+\Delta H$. This time is random because the system is randomly excited. Its statistical moments are given by the solution of the generalized Pontryagin equation (Pontryagin et al., 1989), which is solved according to a stochastic averaging method proposed by Moshchuk (Moshchuk et al., 1995a). The average first passage time $\overline{\tau}_{1}=E[\tau_{1}]$ for this problem is explicitly given by (Vanvinckenroye and Denoël, 2017a)

$$\overline{\tau}_{1}=\frac{4}{S_{u}}\ln\left(\frac{H_{c}S_{u}+2S_{w}}{H_{0}S_{u}+2S_{w}}\right)=\frac{4}{S_{u}}\ln\left(1+\frac{\Delta H^{\star}}{H_{0}^{\star}+1}\right) \tag{11}$$

where the dimensionless groups

$$H_{0}^{\star}=\frac{H_{0}S_{u}}{2S_{w}}\quad\text{and}\quad\Delta H^{\star}=\frac{\Delta HS_{u}}{2S_{w}} \tag{12}$$

have been introduced to simplify the notations. Expression (11) reveals the existence of three different regimes (Vanvinckenroye and Denoël, 2017a).

Incubation regime (I)

For $\Delta H^{\star}\ll H_{0}^{\star}+1$, the average first passage time is proportional to $\Delta H^{\star}$. This is valid for $\overline{\tau}_{1}\ll 4/S_{u}$ so that an *incubation time* is arbitrarily defined as $\tau_{incub}=1/2S_{u}$ corresponding to the time window during which the average first passage time linearly scales with the energy increase $\Delta H^{\star}$.

Multiplicative regime (M)

For $H_{0}^{\star}\gg 1$, the mean first passage time just depends on the ratio $H_{c}^{\star}/H_{0}^{\star}=(H_{0}^{\star}+\Delta H^{\star})/H_{0}^{\star}$, i.e. by how much the initial energy H_{0} is multiplied to obtain the target energy level H_{c} ; it is independent of the forcing excitation intensity S_{w}.

Additive regime(A)

For $H_{0}^{\star}\ll 1$, the first passage time is independent of $H_{0}^{\star}$. No matter the value of the (relatively small) initial energy H_{0} in the system, provided it is much smaller than $2S_{w}/S_{u}$, it does not influence the expected first passage time. In this regime, the expected first passage time only depends on the increase in energy $\Delta H^{\star}$, in other words on how much energy is added to the initial condition H_{0}.

Fig. 1 (a) shows the level curves of the first passage time $\overline{\tau}_{1}\frac{S_{u}}{4}$, as given by (11), as a function of $H^{\star}$ and $\Delta H^{\star}$, and identifies the three regimes (incubation, additive and multiplicative). The bottom part of the diagram represents the incubation regime (**I**), the left part of the diagram corresponding to the additive regime (**A**) presents horizontal asymptotes as the first passage time is independent of the initial energy level. Finally, the multiplicative regime (**M**) is represented in the right part where the first passage time depends on the relative energy increase $\Delta H^{\star}/H_{0}^{\star}$ and the curves present a unit slope in logarithmic scales. As a consequence of the definition of $H_{0}^{\star}$ and $\Delta H^{\star}$, see (12), the forced-only ($S_{u}=0$) and parametric-only ($S_{w}=0$) excitations respectively correspond to the bottom left and upper right corners of this parameter space. They happen to take place in the incubation and multiplicative regimes, respectively. The additive regime can only be accessed with a combination of forced and parametric excitations.

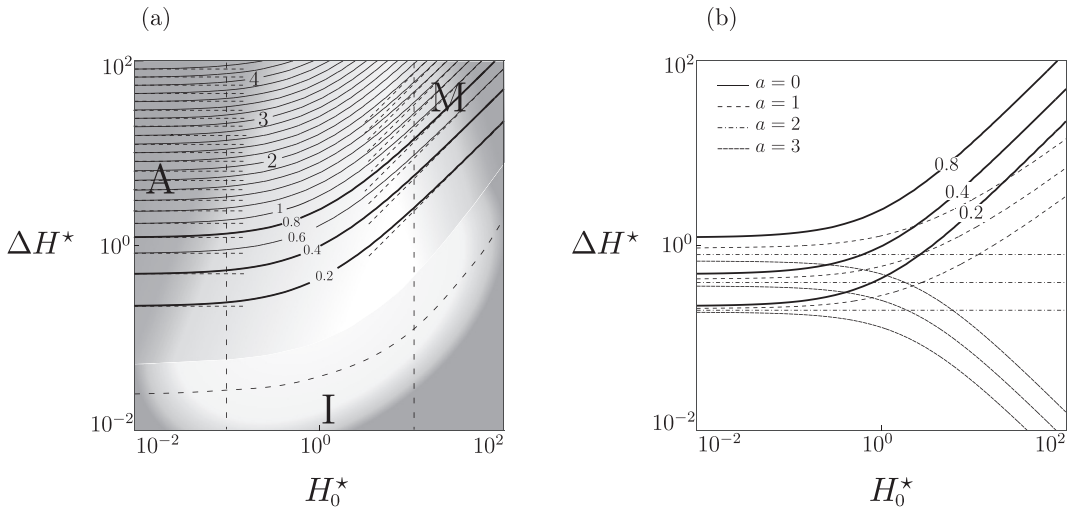

Fig. 1. (a) Representation of the average first passage time $\frac{\bar{\tau}_1 S_u}{4}$ with identification of the three regimes with no damping and (b) with different damping ratios.

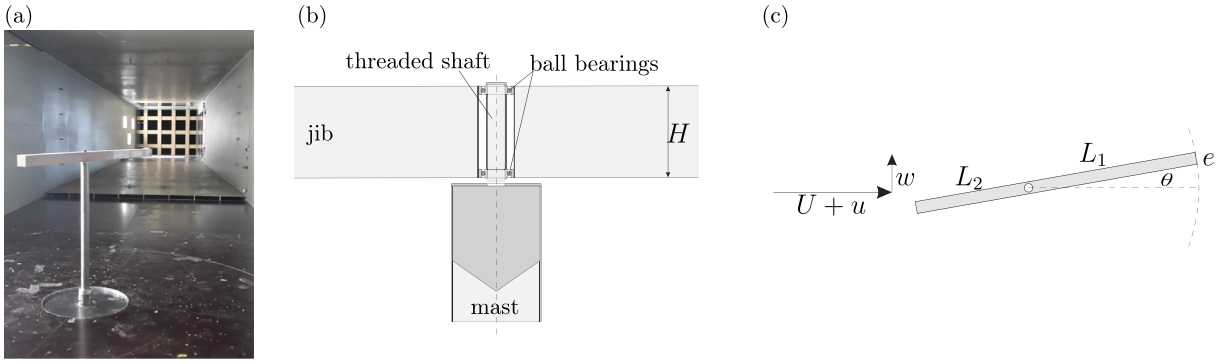

Fig. 2. (a) Experimental setup in the wind tunnel (b) Vertical view and mechanical conception of the pivot (c) Plan view of the setup configuration.

These three behavioural regimes can also be observed in higher order moments. For instance, a closed-form expression of the standard deviation of the first passage time is also available in the undamped case (Vanvinckenroye and Denoël, 2017b). It is not reported here.

Particularisation of expression (11) to the non-dimensional tower crane governing equation (7) provides the non-dimensional first passage time:

$$\bar{\tau}_1 = \frac{4}{S_{\ddot{u}}} \ln\left(1 + \frac{\Delta\tilde{H}}{\tilde{H}_0 + \frac{2S_{\dot{w}}}{S_{\ddot{u}}}}\right). \tag{13}$$

Observing that $S_{\alpha u}(\kappa = \omega/\Omega^\star) = \alpha^2 \Omega^\star S_u(\omega)$ for any real constant α, the average first passage time of the governing equation (5) is finally

$$\bar{t}_1 = \frac{\bar{\tau}_1}{\Omega^\star} = \frac{1}{S_{u/U}\Omega^{\star 2}} \ln\left(1 + \frac{\frac{\Delta H}{M^\star}}{\frac{H_0}{M^\star} + \frac{S_{w/U}}{2S_{u/U}}}\right). \tag{14}$$

3.2. Damped oscillator

A variant of the system, including damping, is governed by

$$\ddot{x} + 2\xi\dot{x} + (1+u)x = w, \tag{15}$$

with ξ a small damping ratio. In this case, the expected first passage time takes a more involved formulation (Vanvinckenroye and Denoël, 2017a),

$$\bar{\tau}_1(H_0) = \frac{4}{S_u(1-a)}\left[\ln\left(1 + \frac{\Delta H^\star}{H_0^\star}\right) + \frac{\left(1 + H_0^\star + \Delta H^\star\right)^a - \left(1 + H_0^\star\right)^a}{a} - \int_{H_0^\star}^{H_0^\star + \Delta H^\star} \frac{(1+z)^a}{z} dz\right] \tag{16}$$

with $a = \frac{8\xi}{S_u}$. Damping enters in the average first passage time only through its ratio with the dimensionless intensity of the parametric excitation. As $a \to 0$, the first passage time given by (16) regularly tends towards (11). This solution is only valid for positive first passage times, which correspond to systems with a limited damping so that energy increases on average (Vanvinckenroye and Denoël, 2017a). When there is no forcing term, *i.e.* $S_w = 0$ (multiplicative regime), the solution degenerates into $\bar{\tau}_1(H_0) = \frac{4}{S_u(1-a)} \ln\left(1 + \frac{\Delta H^\star}{H_0^\star}\right)$. In this case, the damping does not modify the form of the first passage time, which still increases like the logarithm of the ratio H_c/H_0. This solution presents a positive first passage time for $a < 1$, which means that the energy of the system increases, on average, only if the damping ratio is below a certain threshold, $\xi < S_u/8$. For $a \geq 1$, the dissipation mechanism drives the dynamical system to lower energy levels, on average. The evaluated expected first passage time is negative. It has no meaning anymore since the Itô formulation on which the developments are based is no more valid. For a damping ratio equal to the critical threshold, the dissipated energy balances the injected energy and the first passage time is not defined (infinite on average).

Fig. 1 (b) shows the reduced expected first passage time $\frac{\bar{\tau}_1 S_u}{4}$ for

different damping ratios. It is seen that the damping ratio has little influence on the first passage time in the incubation regime (at short time), while it extends the expected first passage time in the additive regime. In the multiplicative regime (upper right corner), the slope of the level curves of the first passage time is affected by the damping ratio; they are still asymptotically linear in the log-log space, which means that the first passage time is governed by a power of $\Delta H^\star/H_0^\star$ smaller than unity. In all regimes, increasing the damping ratio increases the first passage time.

Particularisation of expression (11) to the non-dimensional tower crane governing equation (7) provides the non-dimensional first passage time:

$$\bar{\tau}_1 = \frac{4}{S_{\tilde{u}}(1-a)}\left[\ln\left(1+\frac{\Delta\tilde{H}}{\tilde{H}_0}\right)+\frac{\left(1+\left(\tilde{H}_0+\Delta\tilde{H}\right)\frac{S_{\tilde{u}}}{2S_{\tilde{w}}}\right)^a-\left(1+\tilde{H}_0\frac{S_{\tilde{u}}}{2S_{\tilde{w}}}\right)^a}{a}\right.$$
$$\left.-\int_{\tilde{H}_0}^{\tilde{H}_0+\Delta\tilde{H}}\frac{\left(1+z\frac{S_{\tilde{u}}}{2S_{\tilde{w}}}\right)^a}{z}dz\right] \tag{17}$$

with $a = \frac{8\xi_s}{S_{\tilde{u}}}$. The corresponding dimensional formulation provides the dimensional time $\bar{t}_1 = \Omega^{\star-1}\bar{\tau}_1$

$$\bar{t}_1 = \frac{1}{S_{u/U}(1-a)}\frac{1}{\Omega^{\star 2}}\left[\ln\left(1+\frac{\Delta H}{H_0}\right)\right.$$
$$+\frac{\left(1+\frac{H_0+\Delta H}{M^\star}\frac{2S_{u/U}}{S_{w/U}}\right)^a-\left(1+\frac{H_0}{M^\star}\frac{2S_{u/U}}{S_{w/U}}\right)^a}{a} \tag{18}$$
$$\left.-\int_{H_0}^{H_0+\Delta H}\frac{\left(1+\frac{z}{M^\star}\frac{2S_{u/U}}{S_{w/U}}\right)^a}{z}dz\right]$$

where a can also be expressed as a function of the problem parameters as $a = \frac{C}{IS_{u/U}}\frac{1}{\Omega^{\star 2}} = \frac{2\xi_s}{S_{u/U}\Omega^\star}$.

There are two discrepancies between this mathematical model and the simple tower crane model introduced in Section 2. First, the theoretical solutions are derived for delta-correlated noises $u(t)$ and $w(t)$. In the considered problem, the power spectral densities of the turbulence components are assumed to be broad enough in the frequency bands associated with the dynamics of the problem so that a replacement of the actual power spectral density by an equivalent white noise intensity might be operated. This is classical in buffeting analysis (Davenport, 1962) and has also been discussed in the scope of first passage times. Second, the problem at hand features a parametric excitation in the velocity-dependent term, see (7). In order to get rid of that term, the pivot of the crane model was chosen close to the aerodynamic center so that $r \ll B$.

4. Experimental investigations

4.1. Experimental setup and identification of the mechanical properties of the model

The tests have been performed at the Wind Tunnel Laboratory of the University of Liège, in the low speed test section of dimensions $2.5m \times 1.8m \times 2m$. An homogenous turbulent field is generated $12m$ upstream the tower model using a passive grid generator (Roach, 1987) (see Fig. 3 (a)). The corresponding air flow has been characterized by 3-axis measurement of the wind velocity with a Cobra-probe with an acquisition frequency of $500Hz$. In a first step, long measurements have been performed where the tower crane is left free to rotate in a turbulent velocity field (see Fig. 2 (a)). The rotation of the crane has been measured with a laser SICK OD2-P300W200I0 of range 100 to $500mm$ with an acquisition frequency of $1000Hz$.

The setup consists in a rectangular jib of section $H \times e = 0.042m \times 0.042m$ and length $B = 1m$ made of rigid machinable foam of density $\rho = 690kg/m^3$ (see Fig. 2 (c)). The pivot is placed at $0.4m$ of one extremity so that the jib has a length $L_1 = 0.6m$ and the counter-jib a length $L_2 = 0.4m$ and the inertia is given by $I = \rho He\frac{L_1^3+L_2^3}{3} = 0.11kgm^2$. Friction between the mast and the pivot is minimized by the means of two ball bearings vertically aligned in the pivot as illustrated in Fig. 2 (b). The two ball bearings are adjusted in a circular drilling in the foam. A threaded shaft ensures the verticality and the rigidity of the fixation with the hollow vertical mast.

Finally, the mechanical properties of the physical model have been characterized through measurement of the free response of the crane when it is launched in wind-off conditions. The acceleration has been measured with a wireless PCB accelerometer with acquisition frequency of $200Hz$. The crane has been manually launched in order to observe the free response decay. The corresponding theoretical governing equation is

$$I\ddot{\theta} + C\dot{\theta} = 0. \tag{19}$$

Note that the aerodynamic damping associated with the rotation of the crane is again neglected because of the position of the pivot ($r = 0$). This equation governing the free response of the crane is a particular case of a very general model $\ddot{\theta} + G(\theta,\dot{\theta}) = 0$, where $G(\theta,\dot{\theta})$ is the (possibly nonlinear) restoring force function. In the assumed model, the restoring force function should be a plane independent on the angular position θ. However, slight imperfections in the setup have resulted in a slightly different result, as shown by the surface represented in Fig. 4. This restoring force function has been obtained by measuring the free response of the crane with 3-D accelerometers, then integrating to obtain angular velocity and angular positions. Finally the restoring force function is obtained by plotting the acceleration against the position and velocity. Results shown in Fig. 4 (a) represent an average response over 6 launches. Holes in the map are due to the interpolation algorithm. Fig. 4

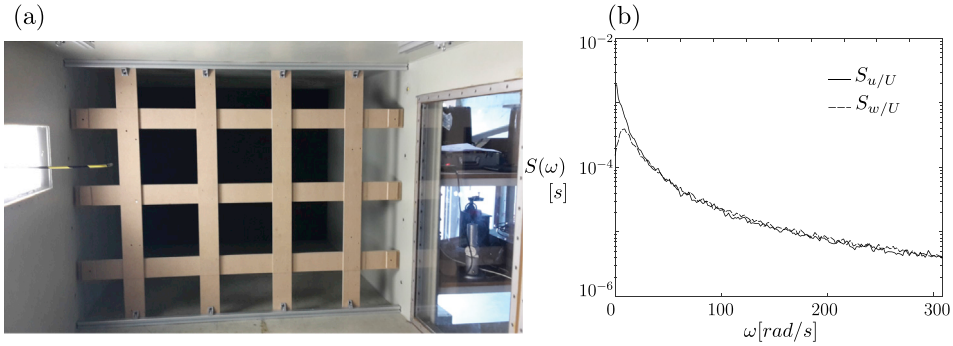

Fig. 3. (a) Coarse grid used for the first passage time measurements (b) Turbulence components parallel (u) and perpendicular (w) to the main wind direction with the coarse grid.

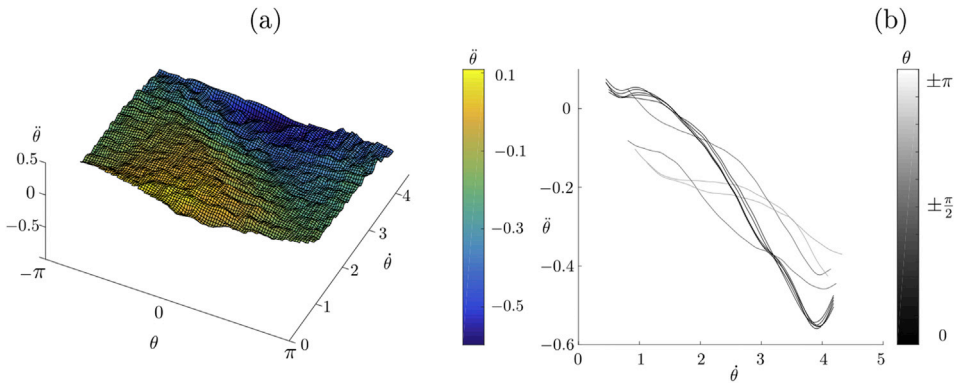

Fig. 4. Representation of the restoring force function as a function of position and velocity (a) and as a function of velocity for $\theta = 0, \pm\frac{\pi}{50}, \pm\frac{\pi}{25}, \pm\frac{\pi}{2}$ and $\pm\pi$ (b).

(b) represents slices of the map for different values of θ.

As expected, an overall decreasing behaviour is observed with $\dot{\theta}$. However, this evolution is slightly nonlinear and dependent on θ. While the acceleration was expected to be always negative due to damping, a small geometrical imperfection influences the acceleration in neighborhood of $\theta = 0$ and for small values of the rotational velocity. For a series of reasons such as small gaps in the ball bearings, small play between the supporting tube and the cylindrical support of the jib (see Fig. 2 (a)), the slight deflection of the jib, and other imperfections, the jib does actually not revolve in a perfectly horizontal plane, creating therefore zones with lower potential energy. These zones are relatively wide and do not hinder the good adjustment of parameters of the linear model, as shown in Section 4.4.

4.2. Grid turbulence

The turbulent field is characterized at a mean velocity $U = 3.6m/s$ and led to horizontal turbulence intensities $I_u = 6.2\%$ and $I_w = 4.8\%$ resp. Parallel and perpendicular to the main direction. The power spectral densities of u/U and w/U are represented in Fig. 3 (b) as a function of the pulsation ω.

The turbulence component u has a monotonically decreasing frequential content while the perpendicular component w presents a peak value for $\omega = 9.1rad/s$. Both contents are very similar for higher frequencies and for all frequencies we have $\mathcal{S}_{w/U}(\omega) \leq \mathcal{S}_{u/U}(\omega)$. The proportional turbulences u/U and w/U characterized here are supposed not to change significantly with the mean velocity U. The Mathieu oscillator is submitted to white noise excitations u and w so that in the next coming results constant values of the spectra $S_{u/U}$ and $S_{w/U}$ are found to be equivalent to the narrow-band spectra $\mathcal{S}_{u/U}(\omega)$ and $\mathcal{S}_{w/U}(\omega)$.

4.3. Algorithmic establishment of the first passage time chart

Fig. 1 shows a chart of the first passage time of the system energy, as a function of the initial energy and of the energy increase. This is an appropriate way to represent the different regimes in which a system could evolve: Incubation, Multiplicative or Additive. In this section, we present an algorithm to determine this chart for measured realizations of the stochastic response.

In practice, the tower crane is left free to rotate under the turbulent flow for 6 hours. Its rotational displacement is measured and the velocity is obtained by differentiation. Then the time series of the dimensionless energy $\tilde{H}(t)$ is established and the first passage time chart as a function of $\tilde{H}_0$ and $\Delta\tilde{H}$ is constructed.

The extraction of first passage times from a time series is composed of several sequential steps. They are explained after some general nomenclature is introduced.

The *main envelope* $\tilde{E}(t; t_0)$ is the monotonically increasing function

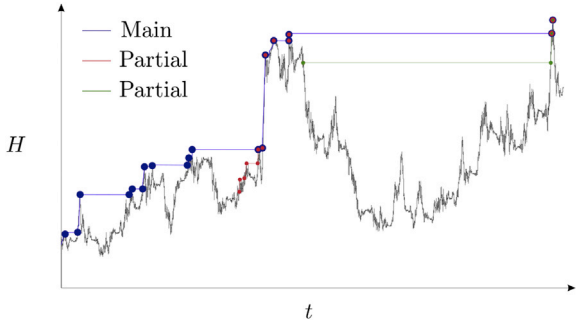

Fig. 5. Main and partial envelopes reconstruction.

corresponding to the highest energy level ever reached at time $t > t_0$. The main envelope is associated with the initial time $t_0 = 0$, where the initial energy is $\tilde{H}_0 = \tilde{H}(0)$, so that $\tilde{E}(t_0; t_0) = \tilde{H}_0$ and $\tilde{E}(t; t_0) \geq \tilde{E}(t_0; t_0), \forall t > t_0$. The main envelope is represented in blue in Fig. 5. This curve provides the target energy levels $\tilde{H}_c = \tilde{E}(t_1; t_0)$ as a function of the corresponding first passage times t_1. The inverse function is not a single-valued function, but if we restrict it to the minimum time corresponding to each energy (i.e. discarding the plateau's in the main envelope), it provides the first passage time as a function of the energy increase $\Delta\tilde{H}$,

$$t_1(\Delta\tilde{H}; \tilde{H}_0) = \tilde{E}^{-1}(\tilde{H}_0 + \Delta\tilde{H}). \tag{20}$$

This time is to be understood as a time elapsed from t_0 where the initial energy is $\tilde{H}_0$. This provides a coarse estimation of the first passage time. A refined estimator can be obtained by pretending that the recording has started a little later, at another time t' where the energy was also equal to $\tilde{H}_0$. By restricting the time series to the window $t > t'$, another estimation of $t_1(\Delta\tilde{H}; \tilde{H}_0)$ is obtained and statistics of the first passage time, starting from initial energy level $\tilde{H}_0$ can be obtained, even from a single realization of the process. The method can be generalized for other values of the initial energy, in such a way to provide a chart of the average first passage time, for various combinations of $\tilde{H}_0$ and $\Delta\tilde{H}$. Nevertheless, it would be computationally ineffective to determine this chart in this way.

For the needs of the following algorithm, we also define the *partial envelope* $\tilde{E}(t; t')$ as the main envelope of the remaining part of the signal starting at time t'. The green and red plots in Fig. 5 show two examples of local envelopes. As a corollary the partial envelope associated with time t_0 corresponds to the main envelope. Unless $\tilde{H}(t')$ is the largest energy level over all times before time t', the local envelope starts below the main envelope and eventually reaches it after some time. The part of the partial envelope that is different from the main envelope is called the *local envelope*.

It is important to notice that the local envelope might coincide with

the time series $\tilde{H}(t)$, depending on the sign of the local derivative at time t'. If the energy $\tilde{H}(t')$ is minimum or increases, then $\tilde{H}(t)$ coincides with the *local envelope* for $t \geq t'$ and until the next local maximum (see beginning of red curve in Fig. 5). On the contrary if the energy presents a maximum or decreases at time t', then the *local envelope* presents a jump until the next point where the energy is higher (see beginning of green curve in Fig. 5).

In order to develop an efficient algorithm, the time series is first scanned through in order to determine, for each time step, whether the energy $\tilde{H}(t)$ is increasing or decreasing. This can be efficiently done with vector operations. For an increasing energy, the index of the next maximum is stored and for a decreasing energy, the index of the next higher energy is stored.

Secondly and using this information, the *main envelope* is constructed, starting from $t = 0$ until the end of the time series (see blue curve in Fig. 5). The main envelope is straightforwardly elaborated as a succession of local envelopes, depending on the ascending or descending character of the signal. The main envelope is stored and will be used as support for the next steps.

Third, the energy axis is discretized in a finite number of intervals. These intervals are chosen with uniform sizes on a logarithmic scale, as this is the physical scaling suggested by the stochastic model. These intervals define bins in the $\tilde{H} - \Delta\tilde{H}$ plane.

Fourth, going point by point through the entire signal, each time step can be considered as the first point $t' \neq t_0$ of a shorter time series with initial energy $\tilde{H}_0' = \tilde{H}(t')$. The *partial envelope* $\tilde{E}(t; t')$ provides estimators of the first passage times t_1 for that initial energy and various target energies (or different energy increases). A counting procedure allocates, in the appropriate bins, the first passage times associated with the target energies, starting from $\tilde{H}_0'(t_0)$. To construct *partial envelopes*, the process is the same, except that the main envelope is now known. If the point $\tilde{H}(t_0)$ is part of the main envelope, then the partial envelope follows the main envelope from that point until the end of the signal. If $\tilde{H}(t_0)$ is not a point of the main envelope, then the envelope is reconstructed as a succession of local envelopes until the main envelope is reached. Once the main envelope is reached, the partial envelope follows the main envelope until the end of the signal.

Finally, since the same discretized energy level will have several occurrences in the original time series, several values of the first passage time will be observed for each $\tilde{H}_0 - \Delta\tilde{H}$ combination (in each bin). Averaging of all these first passage times provides the average first passage time chart.

A pseudo-code of this algorithm, where *main* and *partial* envelopes are established as a succession of *local* envelopes (nested function), is given in Appendix A and Matlab routines are also provided under GNU license, freely available from the website (Vanvinckenroye, 2017).

This algorithm can be seen as a variant of the rainflow algorithm (Downing and Socie, 1982), which is used in fatigue assessment to reduce a varying stress signal into a set of stress reversals and hereby count the number of half-cycles that can lead to fatigue. That algorithm consists in virtually rotating the time signal by 90° and considering a water drop flowing from one point. The path followed by the drop corresponds to our main envelope and provides information about the minima and maxima, as well as an estimation of the number of significant cycles in the signal.

4.4. Results

Fig. 6 (a) shows the chart of the average first passage time reconstructed with the above presented algorithm (in straight line). Dotted lines represent the average first passage times obtained with the mathematical model presented in Section 3. These lines are similar to those of Fig. 1-(b), in the relatively high damped case ($a = 3$). This means that the damping is large compared to the parametric excitation input. It does not mean that damping is large.

While the dimensional problem depends on the four parameters $\Omega^\star$, $S_{u/U}(\omega)$, $S_{w/U}(\omega)$ and ξ_s , see equation (18), the first passage time only depends on three combinations of those 4 parameters: $\frac{1}{S_{u/U}\Omega^{\star 2}}$, $\frac{2S_u}{S_w}$ and a, which means that an infinite number of different oscillators can present the same first passage time chart. In other words, two oscillators that would have two different natural circular frequencies $\Omega^\star$ and subjected to turbulence intensities that are inversely proportional to $\Omega^{\star 2}$, exhibit the same first passage time chart. The faster oscillator being excited with less energetic loadings than the slower oscillator, the energy of both oscillators will actually increase similarly, on average, and they will present the same first passage time chart.

However, the definition of $\tilde{H} = \frac{\theta^2}{2} + \frac{\dot{\theta}^2}{2\Omega^{\star 2}}$ requires the knowledge of $\Omega^\star$, defined as the fundamental pulsation of the time series $\theta(t)$. The characteristic frequency $\Omega^\star = 1.95 rad/s$ has been chosen and obtained as the maximum of the power spectral density of the angular position. This leaves us with the adjustment of 3 parameters.

The parameters of the model are obtained by a minimisation of the mean-square error between the experimental chart and the corresponding theoretical one, defined as

$$\mathcal{R} = \frac{1}{n_1 n_2} \sum_i^{n_1} \sum_j^{n_2} \Delta_{i,j}^2 \frac{N_{i,j}}{N_{tot}} \tag{21}$$

where the summation is repeated over all $n_1 n_2$ bins and where $\Delta = \bar{\mathbf{t}}_{1,exp} - \bar{\mathbf{t}}_{1,th}$ is the difference between the experimental and theoretical $n_1 \times n_2$ matrices of first passage times in the $(H_0, \Delta H)$ space. This error is weighted according to the number of observations $N_{i,j}$ of the first passage time in each bin $N_{tot} = \sum_i \sum_j N_{i,j}$. Implementation of a simple search algorithm provided the lowest residual. The corresponding values of the parameters are

$$S_{u/U} = 3.2 \times 10^{-5} s, \quad S_{w/U} = 6.4 \times 10^{-7} s \quad \text{and} \quad \xi_s = 0.11\,. \tag{22}$$

They correspond to the parameters of the equivalent Mathieu oscillator presented in Section 2. It is not the objective of this work to provide a physical meaning to those parameters. Indeed, they are just equivalent, in the sense of the minimisation (21), since the physical problem tested in the wind tunnel is not exactly governed by the same equation. Although the humble scope of this paper is to highlight a possible field of application of first passage times by exploiting the richness of the generic Mathieu oscillator, it is believed that the direct analysis, i.e. the direct determination of equivalent parameters given all actual properties of the physical problem, goes beyond the scope of this work. We just notice that $S_{u/U}$ and $S_{w/U}$ are short with respect to the timescale of the problem which justifies the slower evolution of energy. Also, we notice that $\xi_s = 0.11$ is a relatively small parameter, which is also a necessary condition for the stochastic averaging to apply. Being defined as a ratio between dissipative moments in the mechanical system and a stationary aerodynamic moment, see (7), the damping coefficient ξ_s has not the classical meaning of a structural nor aerodynamic damping. It is therefore not abnormally large.

Despite the slight dissimilarities between the physical and numerical models, which are emphasized in the next Section, the behaviour in terms of first passage times is very well captured, over several orders of magnitude.

4.5. Discussion

The dimensional incubation time defined as $t_{incub} = \frac{1}{8\Omega^{\star 2} S_{u/U}(1-a)}$ is negative, which means that no incubation regime is observed due to the important structural damping (ξ compared to u/U). The other two regimes are clearly observable: the independence in $\tilde{H}_0$ in the additive regime is observed in the left part of Fig. 6 (a) while the asymptotically constant (and negative) slope which is characterstic of the multiplicative

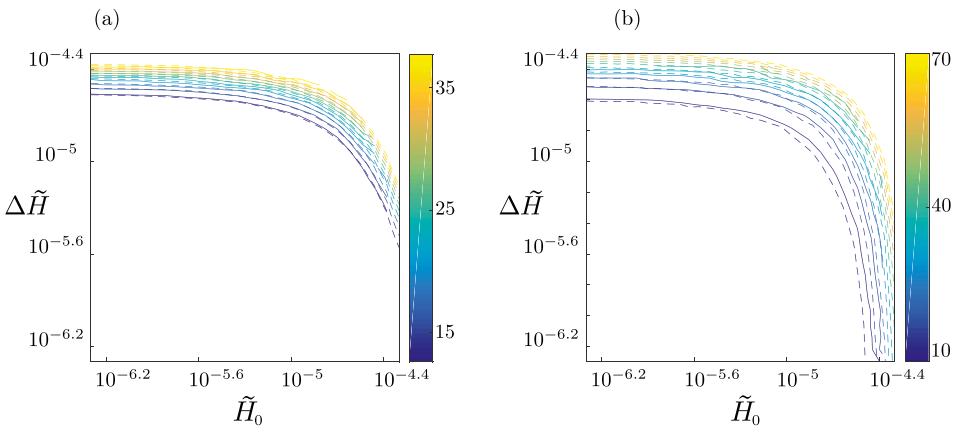

Fig. 6. (a) Charts of the average first passage time $\bar{t}_1$ and (b) of the standard deviation of the first passage time. Comparison between the experimental data (solid lines) and the theoretical model (dotted lines).

regime is observed in the right part of the diagram. The notable change between both behaviours is observed around $\tilde{H}_0 = 10^{-5}$.

The tower crane model is a physical system presenting some differences with the idealized mathematical model of the stochastic Mathieu oscillator of Section 3. First of all, all slight nonlinearities related to the angle of attack, the moment coefficient and the squared apparent velocity have been linearized in order to express the aerodynamic load as a linear function of the turbulence components u and w. Moreover, the quasi-steady model based on the sole consideration of the moment coefficient might be limited to represent the aerodynamic loading on the oscillating crane. Indeed, the aerodynamic moment results from the pressures distributed along the moving jib, which have to be multiplied by their respective lever arms and integrated. These pressures are random as a result of the turbulence, and should in principle be expressed as a slice cut of a spatial stochastic field including the space-coherence of the fluctuating wind. At last but not least, the turbulence components u and w present a broadband spectrum (see Fig. 3 (b)) which is not exactly a δ-correlated noise as assumed in the Mathieu oscillator model. All these reasons conspire to make the actual physical model of the tower crane somehow different from an accurate aerodynamic model of the crane, but also different from the simple Mathieu oscillator model. While the tower crane is a physical problem presenting a significant complexity, to some extent, it is here demonstrated that its first passage behaviour can be captured and reproduced with a simple equivalent model.

This conclusion is very promising as to the utility of simple models to represent first-passage statistic in the buffeting analysis of slightly damped structures. Both the wind-tunnel results and the properties of the equivalent Mathieu oscillator can be exploited to infer some information on the reliability of the considered system. On one hand, very long measurements in the wind tunnel, and the appropriate post-processing in terms of first-passage times, as discussion in Section 4.3, can offer a fair picture of how the first-passage time scales with the problem parameters, in particular, in which regime a randomly excited structure evolves. On the other hand, the adjustment of an equivalent model, as suggested in this paper, can be used to smoothen the slight imperfections of too short measurements or even to extrapolate to situations that could not be observed in the wind-tunnel.

As an example of extrapolation of the information provided by the Mathieu oscillator model, we discuss the standard deviation of the first passage time. This information is as much important as the average first passage time, as soon as reliability is concerned (Vanvinckenroye and Denoël, 2017b). The counting algorithm presented in Section 4.3 can provide additional statistical information about first passage time, including higher statistical moments and the standard deviation. The solid lines in Fig. 6 (b) represent the first-passage time chart of the measured energy. This is now compared to the standard deviation of the first passage time obtained with the Mathieu oscillator model. Unfortunately, the closed form solutions of the second statistical moment are available in the undamped case only (Vanvinckenroye and Denoël, 2017a). However, comparison is possible by means of Monte Carlo simulations. Using the set of parameters obtained by adjusting the mean first passage time, given in (22), we have simulated 10,000 simulations ($dt = 0.01$, and duration as long as required to observe the first passages) of the system, in order to determine the standard deviation of the first passage time. This has resulted in the dotted lines in chart 6 (b). Although a bit less accurate (partly because of looser confidence intervals for higher statistics), there is a fair matching between the measured standard deviation of first passage times and those predicted by the simple model.

As to other possible extrapolations of the model, it is manifestly also a flexible tool to upscale the first passage times measured in the wind tunnel to longer runs. Once a regime (incubation, additive or multiplicative) in which oscillations are taking place is reached, characterized and its boundaries are determined, the analytical model indicates how the first passage time scales with respect to higher energy levels. As long as one is interested in first passage times in this regime, the model might provide fair extrapolations, with all usual limitations of usage on extrapolation.

As a particular example, the model is able to predict for how long measurements would need to be performed in order to reach some larger energy levels. This has two important implications. On one hand, in a preliminary design stage of a wind tunnel setup, the model is able to evaluate for how long the wind tunnel campaign should be foreseen. On the other hand, the model might prove to be a valuable decision tool for those investigators who are already dealing with stability evaluations (Voisin, 2003) and who would like to know whether is it worth prolonging their measurement before larger amplitude might be observed.

5. Conclusion

The first passage time is a tool that is applicable in many wind-engineering problems, especially as soon as the random turbulence of wind is concerned. The closed-form solution of the average first passage time under combined forced and parametric excitations is a quite novel result. It highlighted the existence of various regimes. Among them, the additive and the multiplicative regimes have been observed in the stochastic dynamics of a tower crane in a turbulent flow. This system has been shown to be rather accurately modeled by a simple Mathieu oscillator, at least in terms of first passage times. In this context, this experimental investigation provides a first link between an analytical but simplified result and a more complex reality through the tower crane problem. It is shown that there exists an equivalent linear Mathieu oscillator presenting the same energy evolution from a first passage time point of view. Indeed, average and second-order first passage time charts

are very similar and the theoretical model may be used to understand and predict the tower crane behaviour. A future objective might be the investigation of the different assumptions (white noise excitations, small damping, linearization, no aerodynamic damping) and their impact on the equivalent Mathieu oscillator.

Acknowledgements

H. Vanvinckenroye was supported by the National Fund for Scientific Research of Belgium.

Appendix A. Pseudo-code for the computation of the first passage time chart

Algorithm 1 Construction of the average first passage times chart

Require: $\tilde{H}(t)$
Ensure: FPT, the matrix of average first passage times as a function of $\tilde{H}_0$ and $\Delta\tilde{H}$

Characterization of the time series

for t in time vector **do**
  if $\tilde{H}(t)$ is a minimum or increases in t **then**
    $type(t) = 1$
    $nexttime(t) =$ time of the next maximum
  else
    $type(t) = 2$
    $nexttime(t) =$ time of the next higher value of $\tilde{H}$
  end if
end for

Construction of the main envelope

$t_0 = 0;\ \tilde{H}_0 = \tilde{H}(t_0)$
$t_{local} = t_0$
while $t_{local} < t_{end}$ **do**
  $[\tilde{H}_{local}(t); nexttime] =$ **local**(t_{local})
  $\tilde{H}_c(t) = [\tilde{H}_c(t)\ \tilde{H}_{local}(t)]$
  $t_{local} = nexttime$
end while
$\tilde{H}_c^{main}(t) = \tilde{H}_c(t)$
$\Delta\tilde{H}(t) = \tilde{H}_c(t) - \tilde{H}_0$
$FPT(\tilde{H}_0, \Delta\tilde{H}(t)) = FPT(\tilde{H}_0, \Delta\tilde{H}(t)) + t$
$Counter(\tilde{H}_0, \Delta\tilde{H}(t)) = Counter(\tilde{H}_0, \Delta\tilde{H}(t)) + 1$

Construction of the partial envelopes

for $t_0 = \Delta t : t_{end}$ **do**
  $t_{local} = t_0$
  $\tilde{H}_0 = \tilde{H}(t_0)$
  while $t_{local} < t_{end}$ **do**
    if t_{local} not in main envelope **then**
      $[\tilde{H}_{local}(t); nexttime] = local(t_{local})$
      $\tilde{H}_c(t) = [\tilde{H}_c(t)\ \tilde{H}_{local}(t)]$
      $t_{local} = nexttime$
    else
      $\tilde{H}_c(t) = [\tilde{H}_c(t)\ \tilde{H}_c^{main}(t_{local} : t_{end})]$
      $t_{local} = t_{end}$
    end if
  end while
  $\Delta\tilde{H}(t) = \tilde{H}_c(t) - \tilde{H}_0$
  $t = t - t_0$
  $FPT(\tilde{H}_0, \Delta\tilde{H}(t)) = FPT(\tilde{H}_0, \Delta\tilde{H}(t)) +$
  $Counter(\tilde{H}_0, \Delta\tilde{H}(t)) = Counter(\tilde{H}_0, \Delta\tilde{H}(t)) + 1$
end for
$FPT = FPT./Counter$

Nested function - $local(t_{local})$

Require: t_{local}
Ensure: $\tilde{H}_{local}(t)$, $nexttime$
if $type(t_{local}) = 1$ **then**
  $\tilde{H}_{local}(t) = \tilde{H}(t_{local} : nexttime(t_{local}))$
else
  $\tilde{H}_{local}(t) = \tilde{H}(nexttime(t_{local}))$
end if

References

Alevras, P., Yurchenko, D., Naess, A., 2013. Numerical investigation of the parametric pendulum under filtered random phase excitation. In: Papadrakakis, M., Plevris, V. (Eds.), V. P. (Ed.), Compdyn 2013. Kos Island.

Andrianne, T., de Ville de Goyet, V., 2016. Mitigation of the torsional flutter phenomenon of bridge deck section during a lifting phase. In: 8th International Colloquium on Bluff Body Aerodynamics and Applications. Northeastern University, Boston, Massachusetts, USA.

Barad, M.L., 1958. Project Prairie Grass, a Field Program in Dffusion, vols. I and II. Air Force Cambridge Research Labs Hanscom AFB MA.

Bishop, S., Clifford, M., 1996. Zones of chaotic behaviour in the parametrically excited pendulum. J. Sound Vib. 189 (1), 142–147.

Bolotin, V.V., 1984. Random Vibrations of Elastic Systems. Vol. 8 of Mechanics of Elastic Stability. Springer, Netherlands, Dordrecht.

Canor, T., Denoël, V., 2013. Transient Fokker-Planck-Kolmogorov equation solved with smoothed particle hydrodynamics method. Int. J. Numer. Meth. Eng. 94 (6), 535–553.

Canor, T., Caracoglia, L., Denoël, V., oct 2016. Perturbation methods in evolutionary spectral analysis for linear dynamics and equivalent statistical linearization. Probabilist. Eng. Mech. 46, 1–17.

Carlotta, Costa, Claudio, Borri, nov 2006. Application of indicial functions in bridge deck aeroelasticity. J. Wind Eng. Ind. Aerod. 94 (11), 859–881.

Chopra, A.K., 2007. Dynamics of Structures: Theory and Applications to Earthquake Engineering. [Pearson Education India].

Chunbiao, G., Bohou, X., 2000. First-passage time of quasi-non-integrable-Hamiltonian system. Acta Mech. Sin. 16 (2), 183–192.

Claudio, Borri, Carlotta, Costa, may 2004. Quasi-steady analysis of a two-dimensional bridge deck element. Comput. Struct. 82 (13–14), 993–1006.

Clifford, M., Bishop, S., may 1994. Approximating the escape zone for the parametrically excited pendulum. J. Sound Vib. 172 (4), 572–576.

Davenport, A.G., 1962. Buffeting of a suspension bridge by storm winds. J. Struct. Div. ASCE 88, 233–264.

de Sa Caetano, E., 2007. Cable vibrations in cable-stayed bridges. In: Engineering, I.A.f.B. (Ed.), Structural Engineering Document. IABSE-AIPC-IVBH, p. 188.

Di Sabatino, S., Buccolieri, R., Salizzoni, P., 2013. Recent advancements in numerical modelling of flow and dispersion in urban areas: a short review. Int. J. Environ. Pollut. 52 (3/4), 172.

Downing, S., Socie, D., jan 1982. Simple rainflow counting algorithms. Int. J. Fatig. 4 (1), 31–40.

Dyrbye, C., Hansen, S.O., 1997. Wind Loads on Structures. John Wiley & Sons.

Eden, J., Iny, A., Butler, A., jul 1981. Cranes in storm winds. Eng. Struct. 3 (3), 175–180.

Eden, J.F., Butler, A.J., Patient, J., 1983. Wind tunnel tests on model crane structures. Eng. Struct. 5 (4), 289–298.

Fung, Y.C., 2002. An Introduction to the Theory of Aeroelasticity. Dover Publications.

Garira, W., Bishop, S., 2003. Rotating solutions of the parametrically excited pendulum. J. Sound Vib. 263 (1), 233–239.

Giles, M.B., jun 2008. Multilevel Monte Carlo path simulation. Oper. Res. 56 (3), 607–617.

Gitterman, M., 2010a. Spring pendulum: parametric excitation vs an external force. Phys. Stat. Mech. Appl. 389 (16), 3101–3108.

Gitterman, M., 2010b. The Chaotic Pendulum. World Scientific Publishing.

Gousseau, P., Blocken, B., Stathopoulos, T., van Heijst, G., jan 2011. CFD simulation of near-field pollutant dispersion on a high-resolution grid: a case study by LES and RANS for a building group in downtown Montreal. Atmos. Environ. 45 (2), 428–438.

Grigoriu, M., 2002. Stochastic Calculus: Applications in Science and Engineering. Springer Verlag, Birkhäuser.

Gurley, K.R., Tognarelli, M.A., Kareem, A., 1997. Analysis and simulation tools for wind engineering. Probabilist. Eng. Mech. 12 (1), 9–31.

Halitsky, J., 1963. RP-27–Gas Diffusion Near Buildings. Tech. rep.

Huber, A., Snyder, W., 1982. Wind tunnel investigation of the effects of a rectangular-shaped building on dispersion of effluents from short adjacent stacks. Atmos. Environ. 16, 2837–2848.

Kloeden, P.E., Platen, E., 1992. Numerical Solution of Stochastic Differential Equations. Spring Verlag, Heidelberg.

Kougioumtzoglou, I.A., Spanos, P.D., sep 2014. Nonstationary stochastic response determination of nonlinear systems: a wiener path integral formalism. J. Eng. Mech. 140 (9), 04014064.

Kougioumtzoglou, I.A., Spanos, P.D., 2014. Stochastic response analysis of the softening Duffing oscillator and ship capsizing probability determination via a numerical path integral approach. Probabilist. Eng. Mech. 35, 67–74.

Li, W.-W., Meroney, R.N., jun 1983. Gas dispersion near a cubical model building. Part I. mean concentration measurements. J. Wind Eng. Ind. Aerod. 12 (1), 15–33.

Lin, Y.K., Cai, G.Q., 2004. Probabilistic Structural Dynamics: Advanced Theory and Applications. McGraw-Hill.

Mallick, K., Marcq, P., 2004. On the stochastic pendulum with Ornstein-Uhlenbeck noise. J. Phys. Math. Gen. 37 (17), 14.

Meroney, R., 2004. Wind tunnel and numerical simulation of pollution dispersion: a hybrid approach. In: Paper for Invited Lecture at the Croucher Advanced.

Meroney, R.N., feb 2016. Ten questions concerning hybrid computational/physical model simulation of wind flow in the built environment. Build. Environ. 96, 12–21.

youtube1 Youtube.com Mok, K., 2008. Crane Spinning Out of Control. www.youtube.com/watch?v=6h5p9WC6Y7s.

Moshchuk, N., Ibrahim, R., Khasminskii, R., Chow, P., 1995. Asymptotic expansion of ship capsizing in random sea waves-I. first-order approximation. Int. J. Non Lin. Mech. 30 (5), 727–740.

Moshchuk, N.K., Ibrahim, R.A., Khasminskii, R.Z., Chow, P.L., 1995. Ship capsizing in random sea waves and the mathematical pendulum. IUTAM Symp. Adv. Nonlin. Stoch. Mech. 47, 299–309.

Náprstek, J., Král, R., jun 2014. Finite element method analysis of Fokker-Plank equation in stationary and evolutionary versions. Adv. Eng. Software 72, 28–38.

Náprstek, J., Král, R., jan 2017. Evolutionary analysis of Fokker-Planck equation using multi-dimensional finite element method. Proced. Eng. 199, 735–740.

Palleschi, V., Torquati, M.R., oct 1989. Mean first-passage time for random-walk span: comparison between theory and numerical experiment. Phys. Rev. 40 (8), 4685–4689.

Pontryagin, L., Andronov, A., Vitt, A., 1989. Appendix: on the statistical treatment of dynamical systems. In: Moss, F., McClintock, P.V.E. (Eds.), Noise in Nonlinear Dynamical Systems Volume 1. Theory of Continuous Fokker-planck Systems. Cambridge University Press, pp. 329–348.

Preumont, A., 1994. Random Vibration and Spectral Analysis. Kluwer Academic Publishers.

Primožič, T., 2011. Estimating Expected First Passage Times Using Multilevel Monte Carlo Algorithm. MSc in Mathematical and Computational Finance University.

Risken, H., 1996. The Fokker-planck Equation: Methods of Solution and Applications, pp. 63–95.

Roach, P.E., jun 1987. The generation of nearly isotropic turbulence by means of grids. Int. J. Heat Fluid Flow 8 (2), 82–92.

Roberts, J.B., Yousri, S.N., 1978. An experimental study of first-passage failure of a randomly excited structure. J. Appl. Mech. 45 (4), 917.

Schuss, Z., 2010. Theory and Applications of Stochastic Processes. Vol. 170 of Applied Mathematical Sciences. Springer New York, New York, NY.

Spano, P., D'Ottavi, A., Mecozzi, A., Daino, B., Piazzolla, S., jun 1989. Experimental measurements and theory of first passage time in pulse-modulated semiconductor lasers. IEEE J. Quant. Electron. 25 (6), 1440–1449.

Spanos, P.D., Kougioumtzoglou, I.A., oct 2014. Galerkin scheme based determination of first-passage probability of nonlinear system response. Struct. Infrastruct. Eng. 10 (10), 1285–1294.

Spanos, P.D., Kougioumtzoglou, I.A., jan 2014. Survival probability determination of nonlinear oscillators subject to evolutionary stochastic excitation. J. Appl. Mech. 81 (5), 051016.

Stathopoulos, T., Lazure, L., Saathoff, P., Gupta, A., 2004. The Effect of Stack Height, Stack Location and Rooftop Structures on Air Intake Contamination: a Laboratory and Full-scale Study. Tech. rep., IRSST, Quebec.

Stratonovitch, R. L.-., Silverman, R. A., Topics in the Theory of Random Noise. Volume II, Peaks of Random Functions and the Effect of Noise on Relays, Nonlinear Self-excited Oscillations in the Presence of Noise.

Sun, Z., Hou, N., Xiang, H., 2009. Safety and serviceability assessment for high-rise tower crane to turbulent winds. Front. Architect. Civ. Eng. China 3 (1), 18–24.

Tominaga, Y., Stathopoulos, T., nov 2013. CFD simulation of near-field pollutant dispersion in the urban environment: a review of current modeling techniques. Atmos. Environ. 79, 716–730.

Tominaga, Y., Stathopoulos, T., aug 2016. Ten questions concerning modeling of near-field pollutant dispersion in the built environment. Build. Environ. 105, 390–402.

Troesch, A.W., Falzarano, J.M., Shaw, S.W., 1992. Application of global methods for analyzing dynamical systems to ship rolling motion and capsizing. Internat. J. Bifurc. Chaos 02 (01), 101–115.

Vanvinckenroye, H., 2017. Algorithm for the Determination of the First Passage Time Chart. https://orbi.ulg.ac.be/handle/2268/215378.

Vanvinckenroye, H., Denoël, V., 2015. Monte Carlo simulations of autorotative dynamics of a simple tower crane model. In: Proceedings of the 14th International Conference on Wind Engineering. Porto Alegre, Brazil.

Vanvinckenroye, H., Denoël, V., 2016. Stochastic rotational stability of tower cranes under gusty winds. In: 6th International Conference on Structural Engineering, Mechanics and Computation. Cape Town, South Africa.

Vanvinckenroye, H., Denoël, V., 2017a. Average first-passage time of a quasi-Hamiltonian Mathieu oscillator with parametric and forcing excitations. J. Sound Vib. 406, 328–345.

Vanvinckenroye, H., Denoël, V., 2017b. Second-order Moment of the First Passage Time of a Quasi-hamiltonian Oscillator with Stochastic Parametric and Forcing Excitations (Manuscript under Review). http://orbi.ulg.ac.be/handle/2268/213521.

Voisin, D., 2003. Etudes des effets du vent sur les grues à tour, "Wind effects on tower cranes". Ph.D. thesis. Ecole Polytechique de l'Université de Nantes.

Voisin, D., Grillaud, G., Solliec, C., Beley-Sayettat, A., Berlaud, J.-L., Miton, A., jun 2004. Wind tunnel test method to study out-of-service tower crane behaviour in storm winds. J. Wind Eng. Ind. Aerod. 92 (7–8), 687–697.

Xu, X., Wiercigroch, M., 2006. Approximate analytical solutions for oscillatory and rotational motion of a parametric pendulum. Nonlinear Dynam. 47 (1–3), 311–320.

Yurchenko, D., Naess, A., Alevras, P., 2013. Pendulum's rotational motion governed by a stochastic Mathieu equation. Probabilist. Eng. Mech. 31, 12–18.